treatment, may not be entirely appropriate for an aromatic ring system from plane point group $2mm$.

The rapid increase of computer memory and computer time upon an increase in n, and inclusion of more terms in the series, complicates the investigation of the applicability of eq 2 for much larger numerical values of n (because of the large number of matrices in each serial expression) and very small values of n (because of the large number of terms required for convergence of the series in eq 4 and 6). However, the extrapolation of this equation would predict that K_e is proportional to $n^{-5/2}$ at large n, which is the result of Stockmayer and Jacobson,[12] and therefore the matrix methodology is not needed at large n. Conversely, at small n the problem can be solved by generation and examination of every conformation of the chain. The methodology described here is useful in the transition region between the domains treatable by discrete enumeration and simple analytical expressions.

One factor that is not included in the present analysis is the rate at which nonexcimer-forming rotational isomers are converted to excimer-forming rotational isomers through the process by which a dihedral angle passes over a conformational energy barrier.[14] The successful rationalization of the I_E/I_M for pyr-$(CH_2)_m$-pyr without explicit inclusion of the dynamics may arise when the dependence of the rate constant for first passage from the nonexcimer to the excimer ensemble is dominated by equilibrium quantities.[8] This situation has been shown to exist in A-B_m-A where B is CH_2 and A is C_6H_5COO.[8]

Acknowledgment. This research was supported by a grant from the donors of the Petroleum Research Fund, administered by the American Chemical Society.

References and Notes

(1) Forster, Th. *Angew. Chem.* **1969**, *81*, 364.
(2) Flory, P. J. *Macromolecules* **1974**, *7*, 382.
(3) Zachariasse, K.; Kuhnle, W. *Physik. Chem. Neue Folge.* **1976**, *101*, 267.
(4) Mendicuti, F.; Viswanadhan, V. N.; Mattice, W. L. *Polymer* **1988**, *29*, 875.
(5) Mendicuti, F.; Patel, B.; Viswanadhan, V. N.; Mattice, W. L. *Polymer* **1988**, *29*, 1669.
(6) Mendicuti, F.; Patel, E.; Waldeck, D. H.; Mattice, W. L. *Polymer* **1989**, *30*, 1680.
(7) Bahar, I.; Mattice, W. L. *J. Chem. Phys.* **1989**, *90*, 6775.
(8) Bahar, I.; Mattice, W. L. *J. Chem. Phys.* **1989**, *90*, 6783.
(9) Flory, P. J.; Suter, U. W.; Mutter, M. *J. Am. Chem. Soc.* **1976**, *98*, 5733.
(10) Suter, U. W.; Mutter, M.; Flory, P. J. *J. Am. Chem. Soc.* **1976**, *98*, 5740.
(11) Mutter, M.; Suter, U. W.; Flory, P. J. *J. Am. Chem. Soc.* **1976**, *98*, 5745.
(12) Jacobson, H.; Stockmayer, W. H. *J. Chem. Phys.* **1950**, *18*, 1600.
(13) Abe, W.; Jernigan, R. L.; Flory, P. J. *J. Am. Chem. Soc.* **1966**, *88*, 631.
(14) Winnik, M. *Acc. Chem. Res.* **1985**, *18*, 73.

Registry No. Pyr(CH_2)pyr, 124400-27-7.

Morphology of Highly Textured High-Density Polyethylene

H. H. Song, A. S. Argon, and R. E. Cohen*

Department of Chemical Engineering, Massachusetts Institute of Technology, Cambridge, Massachusetts 02139. *Received May 8, 1989; Revised Manuscript Received August 4, 1989*

ABSTRACT: High-density polyethylene (HDPE) specimens were subjected to high orientation producing deformations below the melting point by using either a rolling mill or a channel die. After appropriate annealing protocols, the crystallographic and morphological textures were examined by using wide-angle X-ray diffraction pole figures, two-dimensional small-angle X-ray scattering and transmission electron microscopy. Although the two deformation patterns resulted in very similar crystallographic textures, the details of the morphological arrangements of crystalline lamellae were different. Quantitative considerations of the 2-D SAXS patterns led to the conclusion that lamellae that are inclined to the macroscopic orientation direction reflect a shear process within the individual lamellae rather than a rigid rotation inside the surrounding amorphous material.

1. Introduction

Modification of semicrystalline polymers from a spherulitic structure to a single crystal-like structure can be effectively achieved by rolling[1] or by channel-die compression.[2] The microstructural arrangements of such oriented semicrystalline polymers are characteried by determining the orientation of crystallographic planes and by the morphology of lamellar stacks. The spatial distribution of the crystallographic planes (pole density) can be precisely measured by wide-angle X-ray diffraction (WAXD). The lamellar structure and its orientation, on the other hand, can be analyzed by 2-D small-angle X-ray scattering (SAXS). Although 2-D SAXS has been used extensively in the past to reveal the lamellar morphology or so-called long period of oriented polymers, the interpretation of the 2-D SAXS patterns has been controversial.[3-5]

The difficulties in interpretation are partially due to the fact that there is no unique lamellar structure, especially in an oriented polymer, but are also due to the inherent characteristics of the scattering method itself (since it is impossible to determine the electron density function $\rho(r)$ of scattering matter directly from the X-ray data). To overcome this problem, transmissin electron microscopy (TEM) can be used as a complementary method to SAXS. TEM has proven to be very effective in revealing the local lamellar structure, especially of polyethylene (PE) for which an effective staining technique has been developed by Kanig[6] to delineate the inter-

0024-9297/90/2223-0870$02.50/0

lamellar amorphous regions. Several TEM studies utilizing this staining technique to reveal the lamellar structure of rolled PE have been published.[7,8] There have been only a few corresponding studies[9] of the lamellar structure of polymers oriented by channel-die compression, which can give more perfect, quasi-single crystalline textures in relatively bulky specimens; this large specimen size makes the channel die a useful tool in the investigation of the anisotropic plastic behavior of crystallizable polymers.[10]

The principal aim of this investigation was to reveal the lamellar morphology of HDPE oriented by channel-die compression in detail and to compare it with the morphology of HDPE obtained by rolling. A secondary aim was to find a general interpretation of the peculiar 2-D SAXS patterns exhibited by these specimens, using TEM micrographs for guidance.

2. Experimental Details

2.1. Materials and Sample Preparation. The material used in this study was high-density polyethylene supplied by the USI Chemical Co. Its molecular weight was M_w = 55 000, with a polydispersity ratio M_w/M_n of 4.8. The degree of crystallinity based on density measurements was 74%. The polymer pellets were compression molded into certain shapes using a hydraulic press to obtain suitable samples for subsequent orientation. The final orientation of these samples was achieved by channel-die compression and by rolling. In both cases the specimens were oriented at a temperature of 100 °C. The thickness reduction in both cases was $\lambda = 6$ (from 3 to 0.5 mm by rolling and from 6 to 1 cm by channel-die compression). The oriented specimens were subsequently annealed in an unconstrained state for 7 h at 117 °C before characterizing their structures. The oriented and annealed samples had degrees of crystallinity in the range of 80% based on density measurements.

2.2. Transmission Electron Microscopy. Transmission electron micrographs were obtained on a Phillips 300 electron microscope operated at 100 kV. The specimens were stained[11] with chlorosulfonic acid, without using uranyl acetate to enhance the contrast between the amorphous and crytalline layers. After staining, the specimens became dark and very brittle, indicating that the rubbery amorphous part becomes extensively cross-linked in the staining process by the acid. The samples were then microtomed in a LKB ultramicrotome fitted with freshly prepared glass knives.

2.3. X-ray Measurement. The overall orientations of crystallographic planes of the oriented samples were determined by means of an automated computer-controlled Rigaku WAXD system consisting of a pole figure device associated with a wide-angle goniometer coupled to a (Cu radiation) rotating anode X-ray generator operating at 50 kV and 60 mA. The 2-D SAXS measurements were performed with assistance of a separate automated computer-controlled system consisting of a Nicolet 2-D position sensitive detector and a Rigaku rotating anode (40 kV and 30 mA) X-ray generator. The primary beam was collimated by a special two mirror collimator.[12] In this way the X-ray beam could be effectively focused onto a beam stop with a very fine size without losing much intensity. The specimen to detector distance of the SAXS system was 135 cm; the scattered beam pathway between specimen and detector was filled with He gas to minimize attenuation and background scattering.

3. Results and Discussion

3.1. Transmission Electron Microscopy. The superimposed pole figures of the crystallographic planes (200), and (020), and (002) of a typical HDPE specimen after rolling or channel-die compression followed by annealing is shown in Figure 1a. The results show that the crystallographic axes a, b, and c can be uniquely defined against the macroscopic specimen axes as is shown in Figure 1b.

Specimens were stained and microtomed, as described above, such that the thin section is parallel to either the

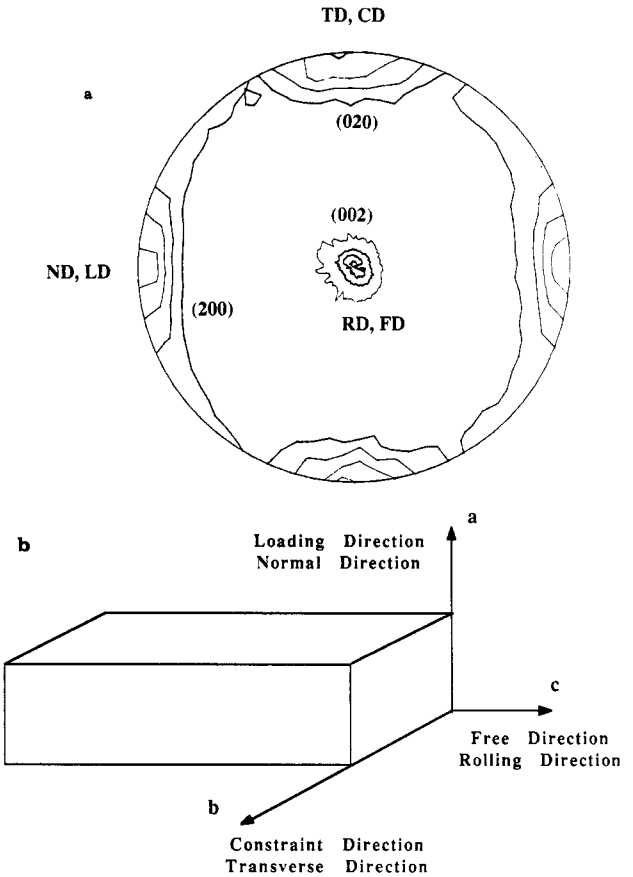

Figure 1. (a) Pole figures of (200), (020), and (002) planes of oriented HDPE by rolling or by channeling-die compression. (b) Schematic diagram of crysallogaphic axes (a, b, c) and macroscopic specimen axes.

(200) plane or the (020) plane. The micrographs thus obtained by TEM are shown in Figures 2a,b and 3a,b. Figures 2a,b and 3a,b are micrographs of a channel-die compressed sample and a rolled sample, respectively. Here Figure 2b and Figure 3b are the micrographs of specimens microtomed parallel to the (200) plane and Figures 2a and 3a are from sections microtomed parallel to the (020) plane. Oriented lamellar stacks are clearly visible in all the micrographs in which black regions represent the stained interlamellar amorphous material. The unusually thick black features suggest either overstaining or swelling of the amorphous layers. Comparing the micrographs of rolled samples with those obtained from channel-die compression, one main feature is apparent. The micrographs of the channel-die sample in Figure 2a,b show remarkably well-ordered lamellar stacks with very large dimensions in both a and b directions, while the rolled sample, shown in Figure 3a,b, shows a corrugated state with relatively smaller lamellar widths of about 1000 Å. Both the rolled and channel-die compression samples, however, show similar features in the lamellar orientation and a comparable interlamellar spacing of about 300 Å. As shown in the micrographs of Figures 2a and 3a, viewed from a direction parallel to the b axis, the lamellar surface normals are tilted with respect to the chain c axis; viewing parallel to the a axis, the long directions of the lamellae are stacked parallel to the b axis (Figures 2b and 3b). Such lamellar orientation suggests that the lamellae are stacked in a sheared state with respect to the flow direction (c-axis direction) mainly on the (200) crystallographic plane.

3.2. 2-D Small-Angle X-ray Scattering. The same specimens were also studied by 2-D SAXS. The pat-

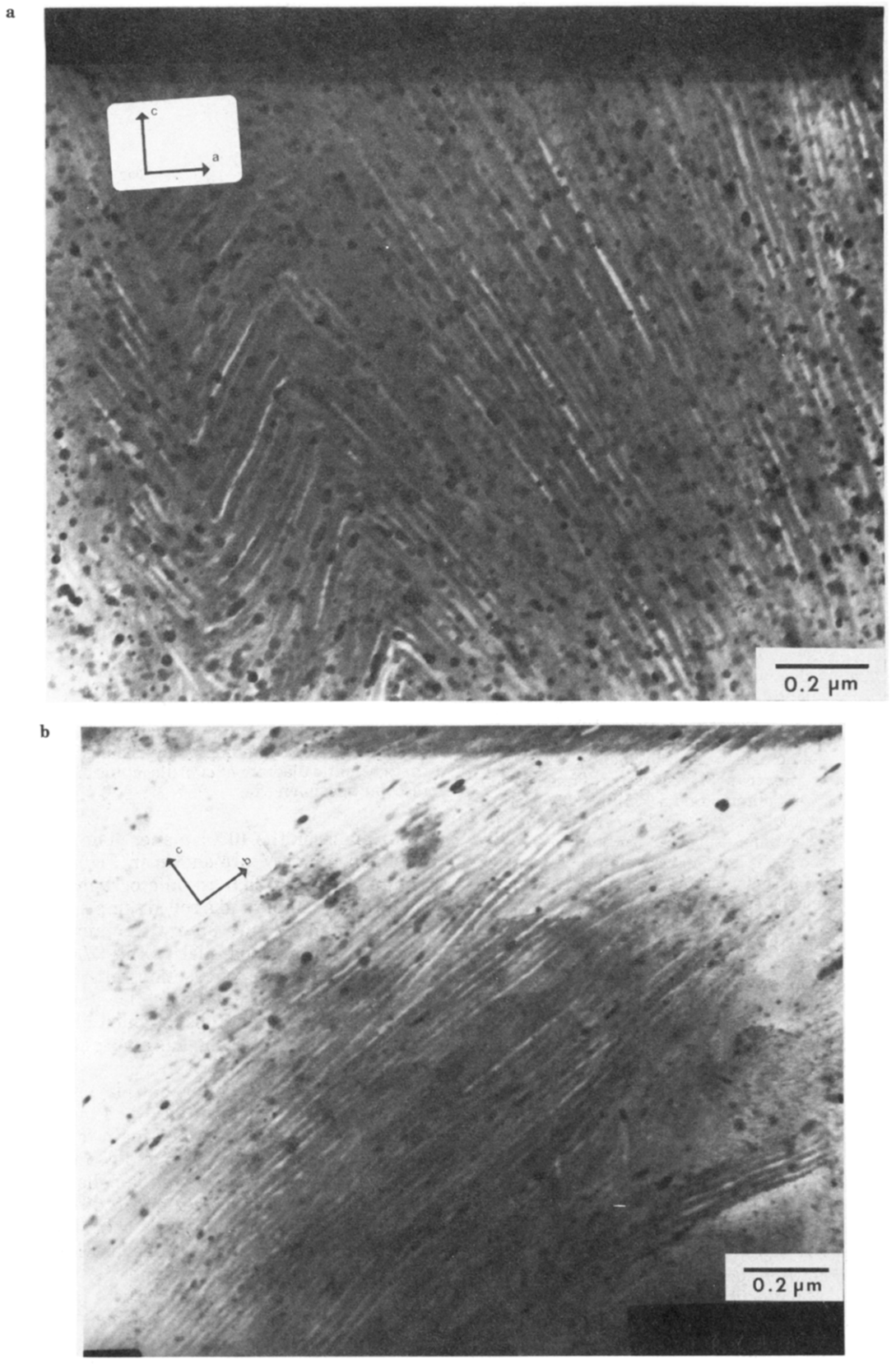

Figure 2. Electron micrographs of channel-die sample: (a) viewed parallel to the *b* axis; (b) viewed parallel to the *a* axis.

terns obtained from the channel-die specimen are shown in Figure 4a–d. Here Figure 4a was obtained with the X-ray beam parallel to the *b* axis. Parts b–d of Figure 4 view the specimen generally in the direction of the *a* axis but are obtained with the specimen rotated around the *b* axis so that the X-ray beam is parallel to the *a* axis (Figure 4b), inclined at 20° with respect to the *a* axis (Figure 4c), and at a 40° inclination with respect to the *a* axis (Figure 4d). Comparison of parts a and b of Figure 4 shows important differences in the SAXS patterns depending on the direction of viewing the specimen; these differences effectively complement the TEM observations presented above.

The diffraction pattern of Figure 4a, obtained with the

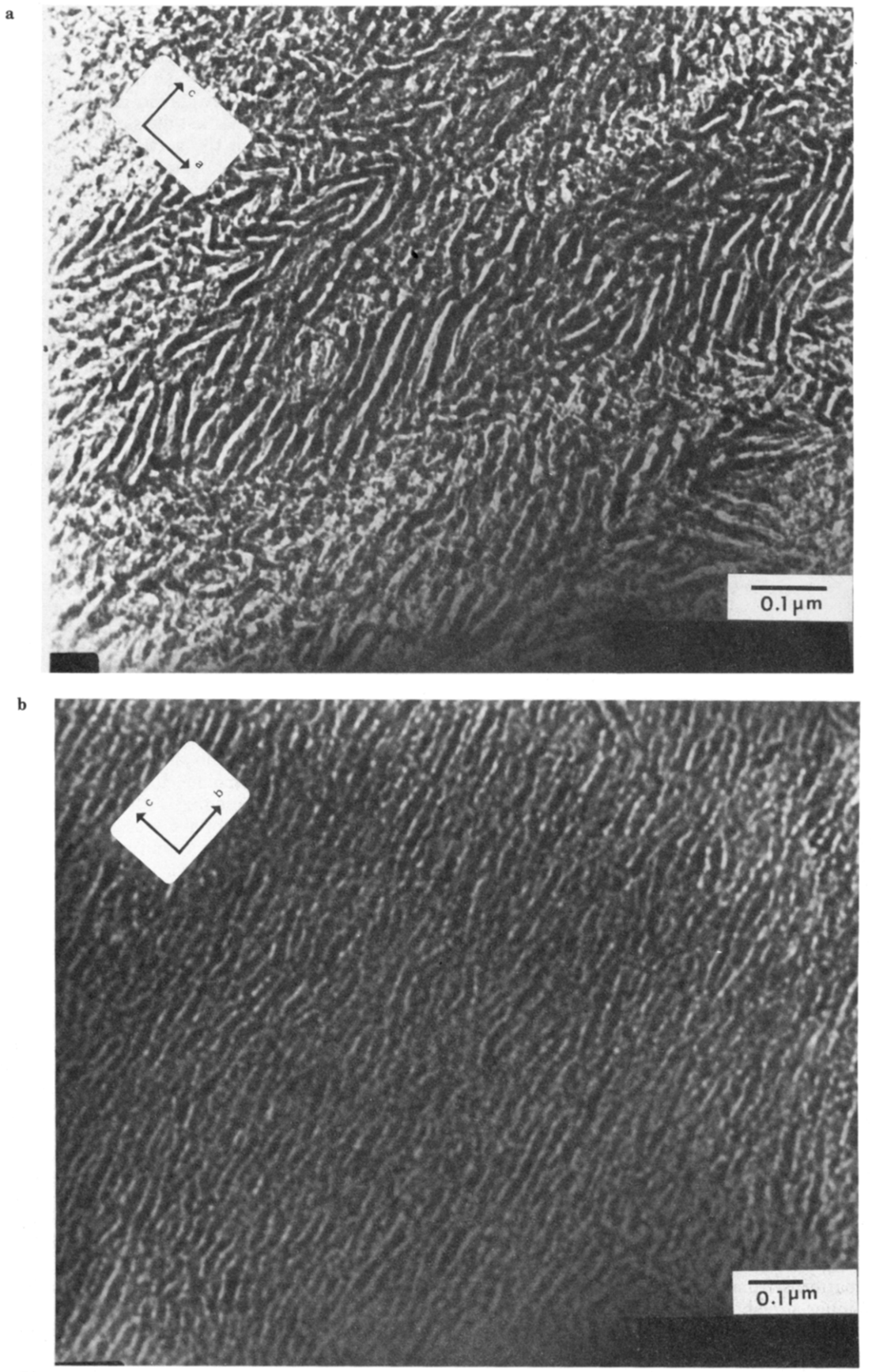

Figure 3. Electron micrographs of rolled sample: (a) viewed parallel to the *b* axis; (b) viewed parallel to the *a* axis.

X-ray beam parallel to the b axis, shows unusually spread out diffraction maxima in the equatorial direction, while the parts b–d of Figure 4 show typical compact point patterns. The interpretation of the origin of such broad small-angle maxima in the equatorial direction has been controversial, since Hess and Kiessig[13] first reported such patterns for hot-stretched polymers. We will discuss our interpretation for such elongated patterns in the next section. We note here that parts b–d of Figure 4 show clearly that the scattering maxima shift to higher angles

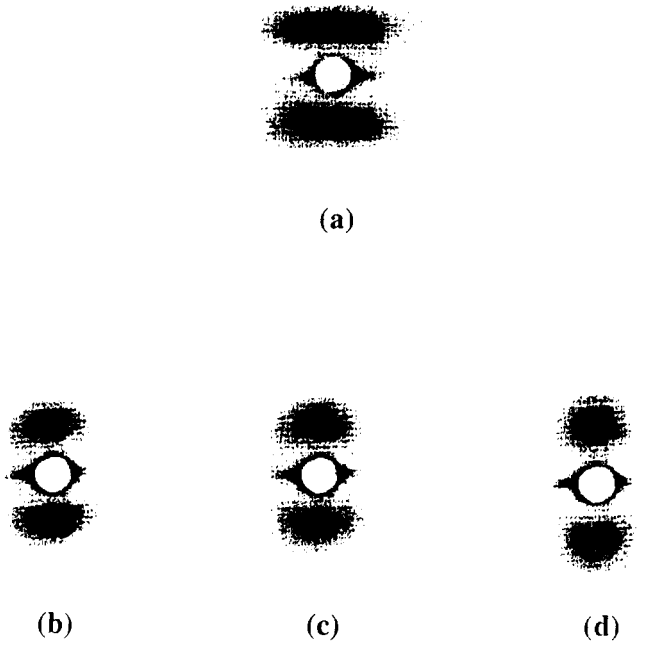

Figure 4. 2-D SAXS patterns of channel-die samples: (a) beam parallel to *b* axis; (b) beam parallel; (c) 20°; (d) 40° to *a* axis.

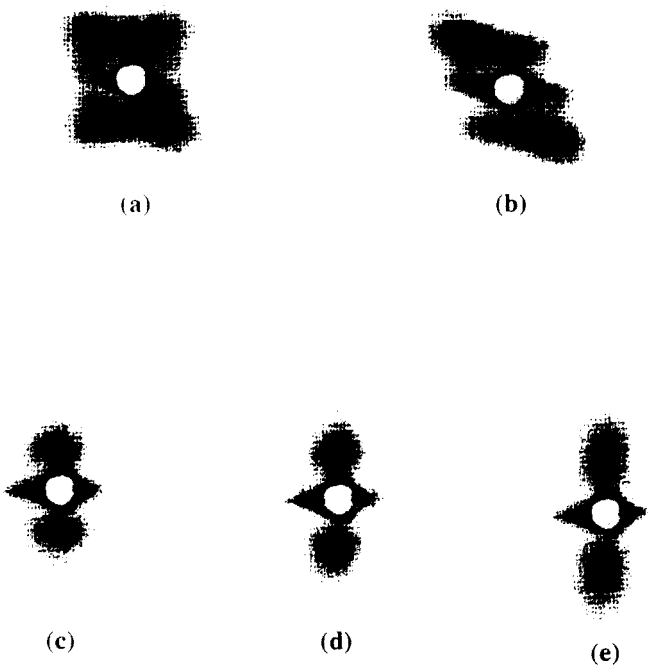

Figure 5. 2-D SAXS patterns of rolled sample: (a) beam parallel to *b* axis and at the center of cross section; (b) at the edge of cross section; (c) beam parallel; (d) 20°; (e) 40° to *a* axis.

with increase in the angle of tilt away from the *a* axis; this means that the lamellar stacks of large tilt with respect to the *a* axis possess smaller spacings. The long spacing obtained from Figure 4a,b is 280 Å.

The SAXS patterns from a rolled sample, measured in a similar manner, are shown in Figure 5a–e. Since it is well-known[1] that in a rolled sample the lamellar orientation varies along the sample cross section, the intensities were measured at the center and at the edge of the sample cross section. Here parts a and b of Figure 5 represent the patterns viewing the samples parallel to the *b* axis: where in Figure 5a, the beam is at the center and is covering the whole cross section of rolled sample, and in Figure 5b the beam is viewing the edge of the cross section. The results show the double lamellar texture with respect to the center line of the cross section as expected.[1] The pattern in Figure 5a, at first glance, appears to be a typical four-point pattern, as often observed by other workers.[1,14] In fact, the dumbbell-like pattern also contains two equatorially spread maxima similar to the one observed in the channel-die sample of Figure 4a but with broader edges in the vertical direction. The patterns obtained with the beam-making angles of 0°, 20°, and 40° with respect to the *a* axis of the rolled specimen are shown in Figure 5c–e. It is interesting to note the SAXS patterns become broader in the vertical direction as well as shifting to the larger angles as the rotation angle with respect to the *x* axis increases. No such broadening effect is observed in the channel-die sample of Figure 4b–d. These results imply that the broad edge in a dumbbell-shaped pattern of Figure 5a, and the vertically spread out patterns of Figure 5d,e are arising from the same lamellar units, as will be discussed further in the next section.

4. Interpretation of the SAXS Patterns

The X-ray diffraction intensity $I(\mathbf{q})$ from a crystal is given by

$$I(\mathbf{q}) = |A(\mathbf{q})|^2 Z(\mathbf{q}) * |S(\mathbf{q})|^2 \quad (1)$$

Here $\mathbf{q}$ is the reciprocal lattice vector, and the asterisk denotes the convolution product. Applying eq 1 to a crystal structure of lamellar stacks, $A(\mathbf{q})$ then represents the structure factor of a single lamellar unit and forms a central scattering pattern at very small angles. $Z(\mathbf{q})$ is the reciprocal lattice function that defines the lamellar periodicity and thus the position of diffraction. $S(\mathbf{q})$ is the form factor, which describes the exterior shape of the lamellar stacks. $A(\mathbf{q})$ and $S(\mathbf{q})$ are determined by the sizes of the scattering units, i.e., single lamellar units for $A(\mathbf{q})$ or bundles of lamellae $S(\mathbf{q})$. These two functions can contribute to broadening of the maxima in either the equatorial or the meridional direction, assuming an ideal lattice function $Z(\mathbf{q})$. For example, maxima are narrow in the meridional direction for large lamellar stacks, and the breadth increases when the size of the stack decreases. Generally, $S(\mathbf{q})$ is a much narrower function than $A(\mathbf{q})$ and therefore the lateral widths of the individual lamellae have been assumed to play the predominant role in equatorial broadening of maxima; this lateral size effect was initially applied by Hess and Kiessig[13] and later by others[14–16] in an attempt to explain the equatorial spread of maxima obtained from oriented semicrystalline polymers. This naturally led to an interpretation that the spread out diffraction spots were due to narrow microfibrils of approximately 100-Å width; the lateral dimensions of such microfibrils can be calculated via Guinier plots[17] of the horizontal intensity profiles of the maxima. Recalling our TEM and SAXS patterns presented above, the conventional interpretation for the horizontal spread of the SAXS spots fails immediately; the lamellar widths seen in TEM are far too large to give such broad maxima in the equatorial direction based on the lamellar width alone (Figures 4a and 5a). Also, the lateral breadths of the SAXS maxima are very different depending on the viewing direction, although the TEM micrographs show comparable lamellar sizes viewed in both *a* and *b* directions. Another interpretation was given by Bonart[18] who attributeed such broadening effects to a paracrystalline layer lattice model[19] with fluctuations of lattice points, $Z(\mathbf{q})$, in the horizontal direction. Applying Bonart's ideas to our data in Figures 4a and 5a, we would have to conclude that the lamellae must be stacked in the meridional direction and that the lamellar surfaces are parallel

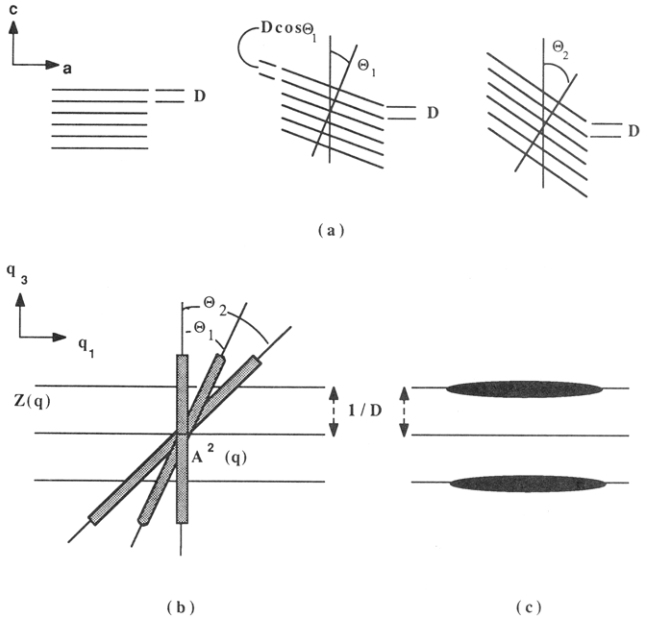

Figure 6. (a) Schematic diagram of 2-D lamellar stacks sheared at different levels. (b) Corresponding $A(\mathbf{q})$ and $Z(\mathbf{q})$ functions. (c) Resulting 2-D small-angle pattern obtained by superposing each pattern.

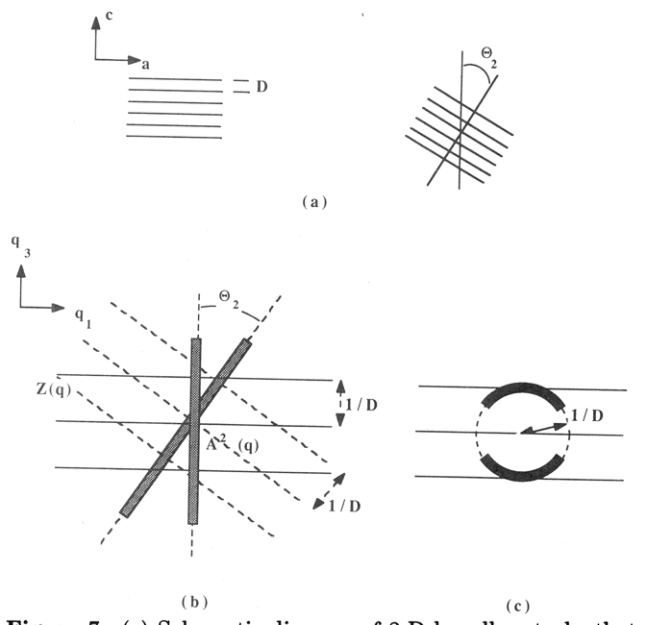

Figure 7. (a) Schematic diagram of 2-D lamellar stacks that are rotated by different amounts relative to the c axis. (b) Corresponding $A(\mathbf{q})$ and $Z(\mathbf{q})$ functions. (c) Resulting 2-D SAXS pattern obtained by superposition.

to the equatorial direction with some degree of fluctuation which determines the lateral breadth of the maxima. However the micrographs of Figures 2a,b and 3a,b reveal entirely different lamellar orientation; the lamellar surface normals are rather tilted with respect to the c axis.

We interpret the broad maxima in the horizontal direction, observed in both the channel-die and rolled samples, as simply a composite of diffraction patterns arising from lamellar stacks sheared at different levels, thus having different lamellar surface angles. Earlier, Point et al.[20] have pointed out the possibility of maxima broadening due to the distribution of lamellar surface angles. Recently, Blöchl and Owen,[8] based on the results of electron micrographs, have applied the same idea to simulate the lateral breadth of 4-point patterns, which showed good agreement with small-angle X-ray results. The schematics shown in Figure 6a,b describe the lamellar stacks with different levels of shear and the corresponding 2-D SAXS pattern expected from these stacks; note that the thickness, $D \cos \theta$, of the individual lamellar crystallite (as measured by the perpendicular distance between its surfaces) decreases as the angle of shear θ increases if we take the distance D to be fixed. This restriction of D is reasonable since it represents a constant HDPE crystalline stem length in the flow direction (recall that the molecular chain c axis and the orientation direction are always parallel (Figure 1a,b) for both channel-die compressed and rolled specimens regardless of the morphological features, including tilted lamellae, seen in the specimens). A constant molecular stem length in the c direction in the crystalline lamellae either could reflect a chain-slip shear process in preformed chain-folded lamellae whose faces were originally perpendicular to the flow direction or could represent a meandering crystallization process in which highly oriented chains crystallize into lamellar stacks in the presence of the stress fields associated with the imposed deformation process. That the observed SAXS patterns are not a result of rigid rotations of lamellar stacks, in which the lamellar thickness perpendicular to the faces remains constant, is eminently clear from Figure 7. Here the shear-free rigid rotation of stacks produces a curved SAXS pattern representing a section of the circular pattern expected from randomly distributed identical stacks, i.e., a powder pattern. Thus we conclude that the SAXS patterns shown in Figures 4a and 5a are superpositions of individual patterns of lamellar stacks with different amounts of shear.

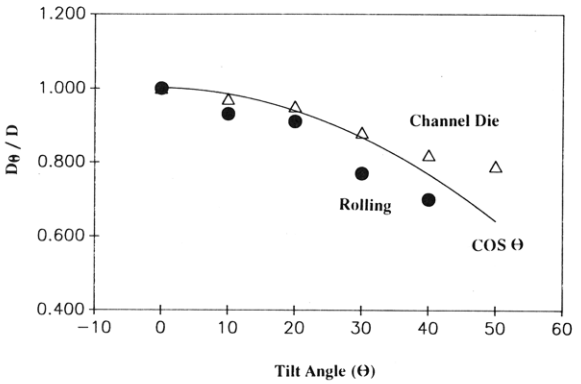

Figure 8. Long spacings of sheared lamellar stacks (D_θ) normalized by D of unsheared parallel stack.

Since the observed small angle diffraction intensity arises only from those particular lamellae that are aligned parallel to the X-ray beam, it is clear that the intensities and spacings should vary as our specimens are rotated around the b axis. Experiments were conducted so that the beam entered the specimen at different angles θ (0–50°) to the a axis, to observe the contributions of those lamellar stacks tilted with the same angle θ to the c axis. Some of the results (θ = 0°, 20°, 40°) were shown in the Figure 4b–d (channel-die compression) and in the Figure 5c–e (rolling). If the constant-stem-length sheared-lamellae model proposed here is correct, the observed spacings from these experiments D_θ should depend on the rotation angle θ as follows

$$D_\theta = D \cos \theta \tag{2}$$

where D is the invariant stem length; D is also the thickness of those lamellae whose normals are exactly parallel (θ = 0) to the c axis or flow direction. Figure 8 is a plot of the normalized long period, D/D_θ, obtained from

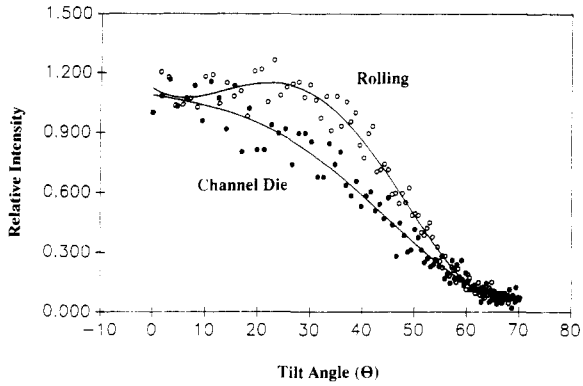

Figure 9. Normalized SAXS intensity vs tilt angle.

these rotation experiments on both the channel-die compressed and rolled specimens, as a function of the rotation angle θ. The agreement with the function cos θ, as anticipated from eq 2, is quite good lending support to the overall interpretations given here.

Finally, some information on the relative populations of lamellar stacks at various angles can be obtained by the equatorial intensity profile of the SAXS maxima. Figure 9 is a plot of normalized intensity profile (relative to I at the center of the maxima) as a function of tilt angle θ for the two types of specimen studied here. The tilt angle θ in the figure is derived from $\cos^{-1}(D_\theta/D)$. Interestingly, the morphological texture, as reflected in the relative amounts of lamellae in each orientation in the material, is quite different for the rolled material and the channel-die compressed specimen. In the former there is some preference for lamellae to lie inclined at 20–30° to the chain c axis, whereas in the channel-die compressed material the relative population of lamellae drops monotonically with angle.

5. Conclusions

Electron micrographs have revealed that two samples of HDPE that were oriented by channel-die compression and by rolling possess distinctly different lamellar morphologies, even though the two samples are very similar in regard to crystallographic orientation relative to macroscopic specimen axes. The channel-die sample showed well ordered lamellar stacks of large dimensions, but the rolled sample showed a corrugated state. Combining the results of micrographs and 2-D SAXS, we conclude that the lamellae in both samples are stacked in a sheared state toward the c axis, so the lamellar surface normals are tilted in the a–c plane. Broad SAXS maxima in the equatorial direction, observed with the beam parallel to the b axis, were then interpreted as a superposition of individual patterns of lamellar stacks sheared at different levels, thus having different surface angles and different lamellar thicknesses.

Acknowledgment. This research was supported by DARPA-URI program under Contract No. N00014-86K0768.

References and Notes

(1) Pope, D. P.; Keller, A. *J. Mater. Sci.* **1974**, *9*, 920.
(2) Gray, R. W.; Young, R. J. *J. Mater. Sci. Lett.* **1974**, *9*, 521.
(3) Cowking, A.; Rider, J. G.; Hay, I. L.; Keller, a. *J. Mater. Sci.* **1968**, *3*, 646.
(4) Groves, G. W.; Hirsch, P. B. *J. Mater. Sci. Lett.* **1969**, *4*, 929.
(5) Hosemann, R.; Loboda-Cackovic, J.; Kaji, K. *J. Appl. Crystallogr.* **1978**, *11*, 540.
(6) Kanig, G. *Kolloid Z. Z. Polym.* **1973**, *251*, 782.
(7) Grubb, D. T.; Dlugosz, J.; Keller, A. *J. Mater. Sci. Lett.* **1975**, *10*, 1826.
(8) Blöchl, G.; Owen, A. J. *Colloid Polym. Sci.* **1984**, *262*, 793.
(9) Burnay, S. G.; Groves, G. W. *J. Mater. Sci.* **1977**, *12*, 1139.
(10) Young, R. J.; Bowden, P. B.; Ritchie, J. M.; Rider, J. G. *J. Mater. Sci.* **1973**, *8*, 23.
(11) Hodge, a. M.; Basset, D. C. *J. Mater. Sci.* **1977**, *12*, 2065.
(12) Franks, A. *Proc. Phys. soc. London* **1955**, *B68*, 1054.
(13) Hess, K.; Kiessig, H. *Z. Phys. Chem.* **1944**, *A193*, 196.
(14) Belbeoch, B.; Guinier, A. *Makromol. Chem.* **1951**, *31*, 1.
(15) Bonart, R.; Hosemann, R. *Kolloid Z. Z. Polym.* **1962**, *186*, 16.
(16) Statton, W. O.; Goddard, G. M. *J. Appl. Phys.* **1957**, *28*.
(17) Guinier, A.; Fournier, G. *Small Angle Scattering of X-rays*; Wiley: New York, 1955.
(18) Bonart, R. *Kolloid Z. Z. Polym.* **1964**, *194*, 97.
(19) Hosemann, R. *Polymer* **1962**, *3*, 349.
(20) Point, J. J.; Homès, G. A.; Gezovich, D.; Keller, A. *J. Mater. Sci.* **1969**, *4*, 908.

Registry No. PE, 9002-88-4.